Low-Dose, Time-Resolved, Contrast-Enhanced 3D MR Angiography in the Assessment of the Abdominal Aorta and Its Major Branches at 3 Tesla

Ulrich Kramer, MD, Michael Fenchel, MD, Gerhard Laub, PhD, Achim Seeger, MD, Bernhard Klumpp, MD, Christiane Bretschneider, MD, J. Paul Finn, MD, Claus D. Claussen, MD, Stephan Miller, MD

Rationale and Objectives: The aims of this study were to evaluate the effectiveness of low-dose, contrast-enhanced (CE), time-resolved, three-dimensional magnetic resonance angiography (MRA) in the assessment of the abdominal aorta and its major branches at 3 T and to compare the results with those of high–spatial resolution CE MRA.

Materials and Methods: Twenty-two consecutive patients (eight men, 14 women; mean age, 43.9 ± 17.9 years) underwent CE time-resolved three-dimensional MRA and high–spatial resolution three-dimensional MRA. Studies were performed using a 3-T magnetic resonance system; gadolinium-based contrast medium was administered at a dose of 3 to 5 mL for time-resolved MRA, followed by 0.1 mmol/kg gadopentetate dimeglumine for single-phase CE MRA. For analysis purposes, the abdominal arterial system was divided into 11 arterial segments, and image quality as well as the presence and degree of vascular pathology were evaluated by two independent magnetic resonance radiologists.

Results: A total of 242 arterial segments were visualized with good image quality. Time-resolved MRA was able to visualize the majority of arterial segments with good definition in the diagnostic range. Vascular pathologies (stenosis, occlusion) or abnormal vascular anatomy was detected in 19 arterial segments, with good interobserver agreement (κ = 0.78). All image findings were detected with time-resolved CE MRA by both observers and were confirmed by correlative imaging.

Conclusion: Low-dose, time-resolved MRA at 3 T yields rapid and important anatomic and functional information in the evaluation of the abdominal vasculature. Because of its limited spatial resolution, time-resolved MRA is inferior to CE MRA in demonstrating fine vascular details.

Key Words: Magnetic resonance angiography; high magnetic field strength; 3 Tesla; time-resolved MRA; parallel imaging technique.

Three-dimensional (3D) contrast-enhanced (CE) magnetic resonance (MR) angiography (MRA) has made substantial technical advances in the past decade and is now widely used in many applications (1–7). Furthermore, CE MRA has been accepted in clinical routine as a substitute for the standard of reference, digital subtraction angiography (DSA), for evaluating the abdominal vasculature and its major branches (1,8–12).

Today most conventional CE MR angiographic methods aim to capture a single imaging volume at peak arterial contrast enhancement with minimal venous overlay. Therefore, these methods require that the acquisition and breath-hold coincide with the presence of the contrast bolus in the vessels of interest for optimal visualization of the arterial tree. But the timing of contrast material arrival may be crucial, because sufficient T1 shortening of blood is achieved only for few seconds during peak vascular concentration. As a result, delayed acquisition will lead to a substantial decrease in diagnostic accuracy. To guarantee accurate bolus timing, different strategies have been developed, including the test-bolus technique (13), automated detection of the contrast material (14), and real-time depiction of bolus arrival (15).

Acad Radiol 2010; 17:564–576

From the Department of Diagnostic and Interventional Radiology, University of Tübingen, Hoppe-Seyler-Straße 3, 72076 Tübingen, Germany (U.K., M.F., A.S., B.K., C.B., C.D.C., S.M.); Siemens Medical Solutions, Malvern, PA (G.L.); and the Department of Radiological Sciences, University of California, Los Angeles, Los Angeles, CA (J.P.F.). Received September 22, 2009; accepted December 9, 2009. **Address correspondence to:** U.K. e-mail: ulrich.kramer@med.uni-tuebingen.de

doi:10.1016/j.acra.2009.12.011

In contrast, "time-resolved" MRA offers combined anatomic and hemodynamic information and obtains pure arterial and venous phase images consistently and rapidly without a timing run (16–19).

At standard field strength of 1.5 T, a trade-off is usually necessary, sacrificing spatial resolution to gain sufficient temporal resolution (4,19–21). With the evolution of k-space acquisition strategies and the introduction of parallel acquisition techniques such as generalized autocalibrating partially parallel acquisitions (GRAPPA) and sensitivity encoding (22,23), time-resolved CE MRA has rapidly emerged as a valuable tool for selected applications to provide dynamic clinical information, including the evaluation of abnormal vascular anatomy as well as vascular hemodynamics and perfusion measurements. To date, useful clinical applications have been shown in the peripheral vasculature, carotid arteries, and pulmonary or aortoiliac arteries (5,17,24–29).

However, abdominal time-resolved CE MRA at 1.5 T remains challenging because of a large volume coverage, limited spatial resolution, and reduced signal-to-noise ratio (SNR) caused by parallel acquisition techniques. With the introduction of MR scanners operating at higher magnetic field strengths, in particular 3 T, for routine MR angiographic applications, the resultant approximate doubling in SNR compared to 1.5-T MR systems can be used to acquire high–spatial resolution and/or high–temporal resolution data sets (4,30–32).

Therefore, the purpose of our study was to evaluate the feasibility and effectiveness of low-dose, CE, time-resolved MRA in the assessment of the abdominal vasculature at 3 T. The results were compared to those of conventional high-resolution 3D CE MRA and catheter angiography when available.

MATERIALS AND METHODS

Patient Population

A total of 22 consecutive patients were prospectively enrolled (eight men, 14 women; mean age, 43.9 ± 17.9 years; age range, 19–66 years) in our study. The inclusion of patients was based on ability and willingness to participate. Clinical indications for MRA were exclusion of renal artery stenosis (RAS) in patients with arterial hypertension (n = 11), evaluation of the abdominal vasculature prior to kidney donation (n = 5), suspicion of fibromuscular dysplasia (FMD; n = 2) on the basis of ultrasound findings, and the assessment of abdominal angina (n = 3) and abdominal aortic aneurysm (n = 1). The study was approved by the institutional review board, and written consent was obtained from all patients.

Patients with contraindications to MR imaging, such as pacemakers, histories of allergic reactions to MR contrast media, or claustrophobia, were not enrolled in this study. On the basis of MR angiographic findings, DSA was performed for further diagnostic clarification or therapeutic reasons in four patients, allowing comparison of both methods in those cases. In those patients, both studies were performed within a range of 0 to 4 days.

MR Imaging

All studies were performed using a 3-T whole-body MR system (Magnetom TimTrio; Siemens Medical Solutions, Erlangen, Germany) equipped with 32 receiver channels and a fast gradient system characterized by a peak gradient amplitude of 45 mT/m and a slew rate of 200 mT/m/ms along each physical axis. For signal reception, a six-element phased-array surface coil was used anteriorly, and six elements of the spine matrix coil were used posteriorly to cover the vasculature from the proximal abdominal aorta to the level of the inguinal ligaments, including the renal and pelvic arteries.

All patients underwent time-resolved 3D CE-MRA first, followed by conventional high–spatial resolution CE-MRA within one single examination without repositioning.

Time-resolved CE MRA

Conventional time-resolved CE MR angiographic techniques on the basis of ultrafast 3D gradient recalled-echo sequences were improved in two ways. A parallel imaging strategy was applied to accelerate data acquisition. Furthermore, a view-sharing imaging technique was applied to scan the center of k-space more frequently than the periphery and to shorten the time between subsequent measurements. This approach is referred to as time-resolved angiography with stochastic trajectories (TWIST). Although detailed physics of the TWIST sequence are beyond the scope of this article, a brief description is provided. The TWIST sequence divides the k-space into a central (A) and a peripheral (B) region. Whereas region A is completely sampled for every measurement repetition, region B is undersampled by a factor of n. The k-space trajectory within region B follows a spiral pattern in the ky-kz plain with every trajectory in B slightly different, depending on the undersampling factor n. During reconstruction, the missing data points in region B for a particular time frame t_i will be copied from the corresponding k-space trajectories in other time frames.

The following sequence parameters were used: repetition time, 2.54 ms; echo time, 1.05 ms; flip angle, 12° to 19° (depending on patient adjustment); sampling bandwidth, 750 Hz/pixel; field of view, 420 × 288 mm^2; matrix size, 512 × 288; 32 partitions with a thickness of 3.8 mm (interpolated to 3 mm); and true voxel size, 1.1 × 0.8 × 3.8 mm^3. A partial Fourier factor of 0.8 was applied in the phase and slice encoding direction to further reduce the acquisition time. Parallel imaging was performed with the GRAPPA algorithm on the basis of the simultaneous acquisition of spatial harmonics and parallel acquisition (27). A GRAPPA acceleration factor of 3 was used, with 24 reference k-space lines for calibration in the left-to-right in-plane phase-encoding direction.

In our study, we used a value of 30% for size A and an undersampling factor of 25% for region B. Therefore, the TWIST acquisition provides 2.1-fold acceleration over a conventional acquisition using similar measurement parameters. Adding the values for parallel imaging and partial Fourier factor, the TWIST acquisition is almost 10 times faster than a standard, full k-space acquisition technique.

To cover the total course of the abdominal aorta and its major branches, a coronal 3D imaging slab was acquired for 14 sequential measurements (one precontrast and 13 postcontrast). Using this imaging approach, a single dynamic scan required 1.7 seconds, and the overall scan time was up to 26 seconds, including the reference scan, which took 5.3 seconds.

Imaging volume positioning was done on a sagittal plane and verified on additional transverse slices. For maximal anatomic coverage, a slab thickness of 9.6 cm was used, with 32 partitions, resulting in an effective partition thickness of 3 mm. The ventral border of the distal aorta was used as a landmark for the anterior extension of the 3D imaging volume. For optimal visualization of the vessels, breath-holding was implemented during image acquisition. No attempt was made to measure the contrast arrival time prior to the scan or to detect the contrast arrival during the scan. The contrast injection protocol consisted of a dose of 3 to 5 mL (depending on patient weight) of gadopentetate dimeglumine (Magnevist; Bayer AG, Leverkusen, Germany) at a rate of 3 mL/s followed by a 30-mL saline flush at the same injection rate (Spectris; Medrad, Inc, Pittsburgh, PA). Patients were instructed to hold their breath in full inspiration as long as possible, and image acquisition was started with a fixed delay of 8 seconds after contrast material injection.

Magnitude subtraction, in the image domain, of the first (unenhanced) data set from all subsequent data sets was performed online, as was on-axis maximum-intensity projection (MIP) reconstruction. Therefore the subtracted images, unsubtracted images, and MIPs of each phase were available for immediate viewing.

Single-phase CE MRA

Subsequently, high–spatial resolution single-phase CE MRA was performed, using a centrically reordered 3D spoiled gradient recalled-echo sequence (repetition time, 2.97 ms; echo time, 1.29 ms; flip angle, 19°–23°; matrix size, 410 × 512; sampling bandwidth, 650 Hz/pixel; GRAPPA acceleration factor, 3), following the injection of 0.1 mmol/kg gadopentetate dimeglumine (Magnevist). Depending on patient conditions (eg, size, weight) the field of view ranged from 380 to 420 mm. For a maximum coverage of the vascular anatomy, a 3D slab thickness of 8 to 10 cm was used, with 88 to 96 partitions. Therefore, the in-plane resolution was $\geq$1.0 × 0.8 mm, and the slice thickness was 1.25 mm (interpolated to 1.0 mm). During a total imaging time of 19 seconds, a nearly isotropic interpolated spatial resolution of 0.8 × 0.8 × 1.0 mm^3 was archived. Sequence parameters are summarized in detail in Table 1. Using the time stamps on time-resolved images, the point of time of contrast material arrival in the abdominal aorta was calculated, and patients were asked to hold their breath at end-expiration. Because not all patients can reliably hold their breath for the total imaging time, centric reordering of the k-space was used, because this acquisition scheme reduces artifacts from incomplete breath-holds.

Repeated MR angiographic volumes were acquired during venous and equilibrium phase with separate breath-holds. To reduce the signal of background tissue, a 3D data set was obtained prior to contrast material administration, which served as mask and was subtracted from the arterial phase.

Sequence parameters that had to be changed during the examination to stay within specific absorption rate limits (eg, flip angle) were noted. Demographic data of all patients (eg, age, sex, body weight) were recorded for statistical analysis (Table 2). Finally, single-phase CE MRA was used for comparative analysis with time-resolved CE MRA, serving as an internal standard of reference.

The total examination time of MRI was 25 ± 5 minutes, including patient positioning. In all patients, both time-resolved and conventional 3D CE MRA were successfully performed after uneventful administration of the contrast agent.

Image Analysis

Two MR radiologists, both with experience in interpreting time-resolved CE MRA and abdominal imaging for $\geq$5 and 10 years, independently reviewed the imaging studies, blinded to patient history and identity and to the results of other diagnostic examinations, on a dedicated imaging workstation (Leonardo; Siemens Medical Solutions), on which source, subtraction images, and 3D multiplanar reformatting and MIPs were available.

Both the time-resolved MR angiographic series and static single-phase MR angiographic series were evaluated qualitatively for image quality as well as the presence of artifacts. No quantitative analyses on the basis of SNR or contrast-to-noise ratio measurements were performed. For research purposes, the readers did a side-by-side comparison of both sequences. Because this was a feasibility study, there was no objective to perform calculations of sensitivity and specificity for time-resolved CE MRA in this setting. The observers were instructed to use postprocessed data in the first step. Separate image reading sessions were organized for both observers by the study coordinator, who attended all reading sessions. A standard form was used to collect all relevant data.

Semiquantitative Analysis

For analytic purposes, the arterial system from the abdominal aorta and its major branches were divided to 11 arterial segments: (1) suprarenal aorta, (2) infrarenal aorta, (3) celiac

TABLE 1. Sequence Parameters of Time-resolved CE MRA and High–spatial resolution Single-phase CE MRA

Parameter	Time-resolved 4D CE MRA	Single-phase 3D CE MRA
Orientation	Coronal	Coronal
Repetition time (ms)	2.54	3.0
Echo time (ms)	1.05	1.14
Flip angle (°)	12–19*	19–23*
Slice thickness (mm)	3.0	1.0
FOV read (mm)	420	420
FOV phase (%)	75	75
Base resolution	512	512
Phase resolution (%)	75	80
Slices per slab	32–36*	88–96*
Matrix size	512 × 288	512 × 308
True voxel size (mm)	1.1 × 0.8 × 3.8	1.0 × 0.8 × 1.6
Interpolated voxel size (mm)	0.8 × 0.8 × 3.0	0.8 × 0.8 × 1.0
PAT mode	GRAPPA	GRAPPA
Acceleration factor	3	3
Reference lines	24	24
Bandwidth (Hz/pixel)	750	650
Number of measurements	14–16*	1
Total scan time (s)	26	19

CE, contrast-enhanced; 4D, four-dimensional; FOV, field of view; GRAPPA, generalized autocalibrating partially parallel acquisitions; MRA, magnetic resonance angiography; PAT, parallel acquisition technique; 3D, three-dimensional.

*Depending on patient adjustment.

TABLE 2. Demographic Data of Patient Population

Patient	Age (y)	Height (m)	Weight (kg)	BMI (kg/m^2)	Reason for MRA Referral
1	56	1.52	73	31.60	RAS
2	46	1.75	66	21.55	Abdominal angina
3	59	1.78	90	28.41	RAS
4	40	1.71	83	28.38	RAS
5	19	1.65	60	22.04	RAS
6	63	1.64	61	22.68	RAS
7	37	1.90	77	21.33	RAS
8	51	1.72	83	28.06	KD
9	61	1.67	84	30.12	RAS
10	59	1.69	53	18.56	AAA
11	32	1.86	112	32.37	RAS
12	50	1.63	70	26.35	Abdominal angina
13	66	1.67	79	28.33	KD
14	65	1.80	75	23.15	Abdominal angina
15	33	1.73	70	23.39	RAS
16	58	1.65	63	23.14	RAS
17	63	1.64	62	23.05	RAS
18	52	1.66	86	31.21	RAS
19	26	1.78	83	26.20	KD
20	45	1.77	78	24.90	KD
21	54	1.70	69	23.88	KD
22	27	1.73	55	18.38	FMD

AAA, abdominal aortic aneurysm; BMI, body mass index; FMD, fibromuscular dysplasia; KD, kidney donation; MRA, magnetic resonance angiography; RAS, renal artery stenosis.

artery, (4) common hepatic artery, (5) splenic artery, (6) renal arteries, (7) accessory renal arteries, (8) superior mesenteric artery, (9) inferior mesenteric artery, (10) common iliac arteries, and (11) external iliac arteries.

First, each visualized branch was analyzed with regard to image quality for how clearly the vessel was defined ("visibility score"), using a Likert-type scoring scale ranging from zero to four (0 = impaired image quality, inadequate for diagnosis;

1 = poor image quality and blurring of the arterial segment; 2 = fair image quality but inadequate arterial enhancement for confident diagnosis; 3 = good image quality and arterial enhancement, adequate for confident diagnosis; and 4 = excellent image quality and arterial enhancement, for highly confident diagnosis). The image quality of an arterial segment was rated to be diagnostic (score ≥3) only if all clinically relevant diagnostic information was felt to be confidently visualized by the reviewers.

For comparative analysis, to estimate the diagnostic performance regarding the depiction of each abdominal segment, in the second step, a "total vessel visibility score" was calculated, gradually adding all values. This analysis was done both on a per patient basis and on a per segment basis. According to this, a maximum value of 44 was accessible per patient (11 segments, four points each) and a maximum value of 176 per segment (22 patients, four points each, two reader).

Because most patients were examined for evaluation of arterial hypertension, in the third step, each reader was asked to identify and characterize the presence (or absence) of RAS on time-resolved MR images. Similarly, the presence, type, and severity of artifacts, such as ringing of the parenchyma or motion-introduced blurring of renal arteries, venous overlay, as well as parallel imaging reconstruction artifacts, were recorded for each patient on both sequences using a "level of artifact" scoring system (1 = no artifacts, 2 = present but not affecting image interpretation, and 3 = present and affecting image interpretation).

Correlation with DSA

For MRA, correlation with DSA was possible in four patients. In these four patients, a total of eight main renal arteries and one accessory renal artery were present. On DSA, two severe stenoses of the main renal arteries were found and treated by stent placement. In two renal arteries, FMD-like lesions were found and therefore treated by percutaneous balloon angioplasty.

Statistical Analysis

An unpaired Wilcoxon's rank-sum test was used to determine the significance of the image quality grading differences between the two observers. Interobserver agreement for image quality grading as well as the detection of RAS was also evaluated using κ statistics (poor agreement, $\kappa = 0$; slight agreement, $\kappa = 0.01$–0.2; fair agreement, $\kappa = 0.21$–0.4; moderate agreement, $\kappa = 0.41$–0.6; good agreement, $\kappa = 0.61$–0.8; and excellent agreement, $\kappa = 0.81$–1.0). Correlation between time-resolved CE MRA and single-phase CE MRA in terms of categories of pathologies was calculated using mixed-model regression analysis to account for statistical dependencies among observations provided by each reader for the same patient. The level for a statistically significant difference was set at $P < .05$. All statistical tests were performed using SPSS version 11 (SPSS, Inc, Chicago, IL).

RESULTS

The applied imaging protocol was sufficient to deliver good diagnostic image quality for both sequences in all cases. No study had to be repeated because of technical problems. Time-resolved CE MRA allowed reliable differentiation of the early and main arterial phases and of at least the early venous phase (Fig 1). Furthermore, time-resolved CE MRA was able to visualize the majority of arterial segments with definition in the diagnostic range.

With an imaging delay of 8 seconds between the contrast media injection and the start of the time-resolved imaging, there was at least one nonenhanced phase image in 19 of 22 patients (86%). In the remaining three patients (14%), no nonenhanced phase image was archived, but early arterial phase images were obtained in all studies.

Vascular Pathology

By conventional 3D CE MRA, a total of 242 arterial segments were evaluated in 22 patients. In nine of 22 patients (41%), a total of 12 accessory renal arteries were found, nine (75%) of them located on the right side and three (25%) on the left side. In six patients (27%), RAS ($n = 4$) or FMD-like lesions ($n = 2$) were found; four (18%) of them were referred to DSA for confirmation of MR angiographic findings and/or interventional treatment (percutaneous balloon angioplasty, $n = 2$; stent placement, $n = 2$). In two patients presenting with renovascular pathology, the renal arteries were graded as only mildly stenotic (1%–50%) or moderately stenotic (51%–70%), so medical treatment was continued. One patient (5%) presented with an abdominal aortic aneurysm, and in two patients (9%), stenoses of the celiac trunk causing abdominal angina were found. In the remaining 13 patients (59%), no abdominal-vascular pathology was found using 3D CE MRA (Fig 2). One patient (5%) presented after kidney transplantation; there was no evidence of stenotic vascular anastomosis.

Vessel Depiction and Visibility Score

A complete overview of all vessel scores of both readers can be found in Tables 3 and 4. Both readers considered overall image quality and diagnostic performance with conventional single-phase 3D CE MRA to be higher than those with time-resolved CE MRA. On a per patient basis, the mean vessel visibility score was significantly higher for conventional single-phase CE MRA (38.8 ± 3.07) compared to time-resolved CE MRA (27.8 ± 5.03) (Table 3). There was a good interobserver agreement between readers 1 and 2 ($\kappa = 0.78$) for diagnostic confidence and the conspicuity of vessel segments.

On a per segment basis, both readers found improved depiction of the smaller vessel branches in terms of vessel conspicuity, represented by segment 4 and 5 as well as segments 8 and 9, with single-phase CE MRA compared to time-resolved MRA. Segments 1 to 3, 6, 7, 10, and 11 were almost equally well seen with both techniques, although there

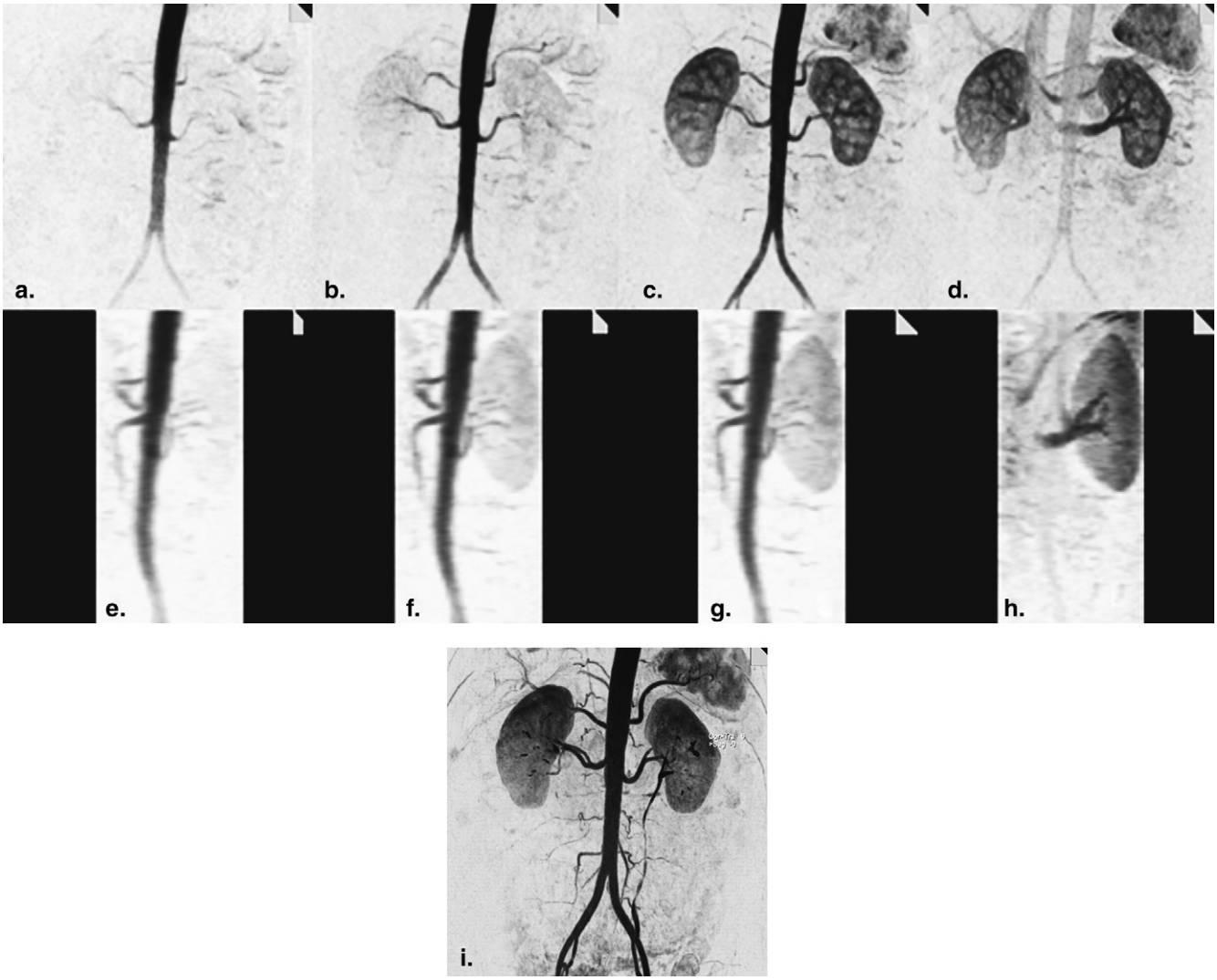

Figure 1. Selected subset of coronal **(a–d)** and sagittal **(e–h)** thin maximum-intensity projection (MIP) images generated during contrast bolus transit. The fast image acquisition technique provides clear separation of arterial, arteriovenous, and beginning venous filling. Only mild venous filling and parenchymal flush can be observed in images **(d)** and **(h)**. Because of high spatial resolution (in-plane, 1.1 × 0.8 mm), early arterial branching (<2 cm) of the right renal artery can be observed. **(i)** High-resolution single-phase MIP image in the same subject, with contrast media in the left urinary system as a consequence of a prior timing run.

was a tendency for lower values on time-resolved data sets for these segments by either reader (Table 4).

Figures 3 and 4 present two examples of time-resolved CE MR angiographic images acquired using the TWIST acquisition and corresponding MIP images from single-phase 3D CE MRA in the same patients; in contrast, particularly with regard to smaller vessel diameters, as in the superior or inferior mesenteric arteries, these segments were significantly better depicted with single-phase 3D CE MRA.

On the basis of single-phase 3D CE MR angiographic findings, six patients presented with RAS and/or FMD. All findings were confirmed by time-resolved 3D CE MRA as well.

Image Artifacts

Both readers found no subjective significant differences with respect to the artifact scoring system between the use of time-resolved and single-phase 3D CE MRA in this study. Accordingly, interobserver agreement was excellent for the assessment of artifacts (κ = 0.86). The time-resolved and conventional MR angiographic data sets, respectively, had mean artifact scores of 1.45 ± 0.5 and 1.27 ± 0.45 for observer 1 and 1.36 ± 0.48 and 1.32 ± 0.47 for observer 2. No statistically significant difference was evident between the scoring of both observers (P = .43 for time-resolved and P = .75 for single-phase CE MRA). The mean levels of artifacts were 1.29 for single-phase 3D CE MRA and 1.41 for time-resolved 3D CE MRA.

Artifacts seen on both sequence types included predominantly motion artifacts. For time-resolved imaging studies, in 10 of 22 patients (45%), blurring of the edges of the vessels secondary to motion was found. Nevertheless, in all these cases the arterial phase was free of motion artifacts. For static single-phase 3D CE MRA, reduced sharpness of vessel borders could

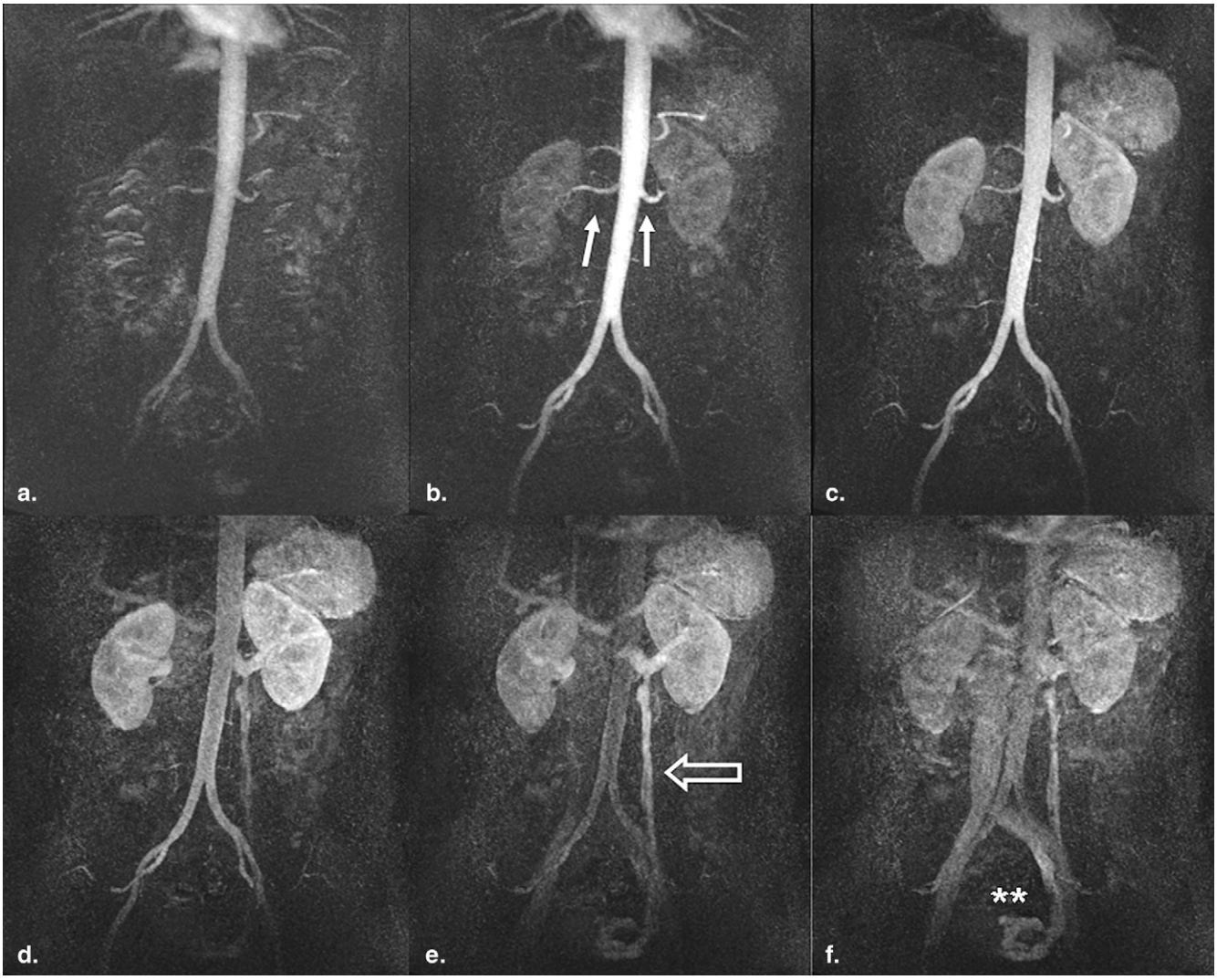

Figure 2. Six consecutive coronal maximum-intensity projection images **(a–f)** from a three-dimensional time-resolved contrast-enhanced magnetic resonance angiographic data set in 43-year-old woman presenting with secondary arterial hypertension. The suprarenal and infrarenal abdominal aorta as well as the renal arteries (b, white arrows) are clearly delineated. In the venous phase, an insufficiency of the left ovarian vein (e and f, open arrow) was found as a secondary finding.

be noticed as a consequence of subtraction artifacts. Neither venous overlay hampering diagnostic image quality nor image reconstruction artifacts related to parallel acquisition techniques were found in any of the patients' images.

DISCUSSION

To our knowledge, this is the first clinical study using the TWIST method of temporal undersampling in combination with parallel imaging and higher field strength to assess the abdominal vasculature. We have shown that with small doses of intravenous contrast, time-resolved CE MRA of the abdominal vasculature at 3 T is feasible, consistently allowing visualization of the entire course of the abdominal aorta, from the diaphragm to the iliac arteries, with good temporal (1.7 seconds) and high spatial (in plane, 1.1×0.8 mm^2) resolution. Our preliminary data demonstrate that the sequence mentioned above can provide MRA of the abdominal vasculature with both high spatial resolution and a high temporal reconstructed frame rate. Four-dimensional imaging capability (3D spatial resolution plus one-dimensional temporal resolution) provides detailed contrast enhancement kinetics and a solution for imaging delayed filling or asymmetric filling of the contrast bolus.

Technical Considerations

Time-resolved acquisition did not require a test bolus, resulting in satisfactory arterial enhancement in all cases. An 8-second imaging delay after the start of the contrast media injection proved to be a reliable and robust way to minimize imaging time prior to contrast material arrival without missing the bolus. None of the time-resolved studies revealed breathing artifacts that affected image analysis substantially,

TABLE 3. Results for Total Vessel Visibility Score on a per Patient Basis Calculated for Both Sequence Types

	Time-resolved 4D CE MRA (TWIST)			Single-phase 3D CE MRA		
Patient	Reader 1	Reader 2	Mean	Reader 1	Reader 2	Mean
1	34	35	34.5	40	39	39.5
2	30	30	30	34	35	34.5
3	26	28	27	40	40	40
4	24	24	24	39	37	38
5	24	23	23.5	33	35	34
6	28	29	28.5	36	36	36
7	21	22	21.5	40	39	39.5
8	25	24	24.5	40	38	39
9	26	26	26	40	40	40
10	25	25	25	44	42	43
11	20	21	20.5	40	40	40
12	35	36	35.5	42	40	41
13	37	36	36.5	41	41	41
14	35	37	36	44	44	44
15	24	25	24.5	31	32	31.5
16	31	32	31.5	42	43	42.5
17	32	31	31.5	39	39	39
18	22	23	22.5	36	38	37
19	19	20	19.5	35	34	34.5
20	28	31	29.5	40	39	39.5
21	29	31	30	40	38	39
22	28	32	30	40	40	40
Maximum	37	37	37	44	44	44
Minimum	19	20	19.5	31	32	31.5
Mean	27.4	28.2	27.8	38.9	38.6	38.8
SD	4.96	5.11	5.03	3.30	2.84	3.07

CE, contrast-enhanced; 4D, four-dimensional; MRA, magnetic resonance angiography; 3D, three-dimensional; SD, standard deviation; TWIST, time-resolved angiography with stochastic trajectories.

The mean visibility score for conventional single-phase 3D CE MRA was significantly higher than for time-resolved multiphase 4D CE MRA.

TABLE 4. Results for Total Vessel Visibility Score on a per Segment Basis Calculated for Both Sequence Types

	Segment																					
	1		2		3		4		5		6		7		8		9		10		11	
	4D	3D	4D	3D	4D	3D	4D	3D	4D	3D	4D	3D	4D	3D	4D	3D	4D	3D	4D	3D	4D	3D
Sum	176	176	175	176	61	167	59	128	125	167	168	174	34	46	63	166	13	153	176	176	174	176
Visibility score																						
0	0	0	0	0	16	0	14	5	3	0	0	0	34	32	18	0	35	4	0	0	0	0
1	0	0	0	0	10	0	13	3	5	0	0	0	0	0	8	0	5	0	0	0	0	0
2	0	0	0	0	7	2	9	5	8	1	1	0	2	0	4	2	4	2	0	0	0	0
3	0	0	1	0	7	5	4	9	8	7	6	2	2	2	9	6	0	3	0	0	2	0
4	44	44	43	44	4	37	4	22	20	36	37	42	6	10	5	36	0	35	44	44	42	44

4D, four-dimensional; 3D, three-dimensional.

Vessel segments with smaller diameters, such as the hepatic artery (segment 5), splenic artery (segment 6), superior mesenteric artery (segment 8), and the inferior mesenteric artery (segment 9), were significantly better shown in detail on single-phase 3D contrast-enhanced magnetic resonance angiography.

because all patients were able to hold their breath at least for the peak arterial and the parenchymal image phases. Breathing artifacts at the venous imaging phases were found in seven studies as a consequence of incomplete breath-holds.

TWIST differs in the trajectory of k-space sampling compared to other temporal undersampling techniques described in the literature, such as time-resolved imaging of contrast kinetics (17) and the time-resolved

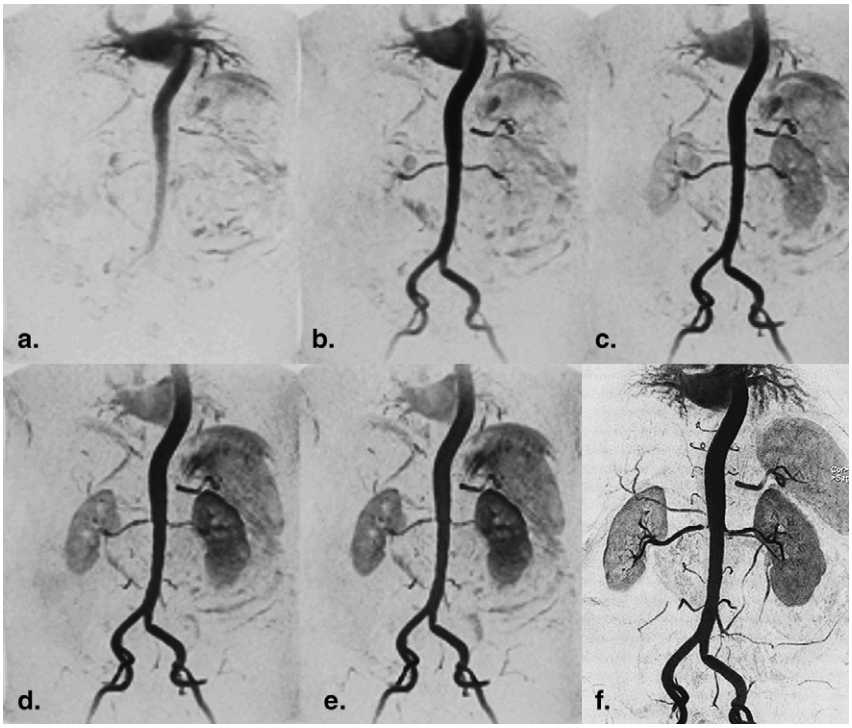

Figure 3. Dynamic inverted maximum-intensity projection coronal **(a–e)** series in a 65-year-old man with arterial hypertension. There is a delayed parenchymal enhancement of the right kidney due to a high-grade renal artery stenosis. **(f)** Comparison to high–spatial resolution contrast-enhanced magnetic resonance angiography. Because of the magnetic resonance angiographic findings, the patient was referred to digital subtraction angiography and successfully treated by stent placement **(g–l)**.

echo-shared angiographic technique (18). TWIST uses a spiral and pseudostochastic rather than a linear trajectory to traverse a full range of k-space with every iteration, from center to periphery, on the basis of radial distance from the center of k-space, with theoretic advantages in image quality and reduction of artifacts.

Furthermore, time-resolved MR angiographic sequences are extremely efficient in terms of amount of anatomic coverage per unit imaging time compared to other sequences. Because subtraction images were available for interpretation, background signal intensity could be eliminated, and the small contrast dose used for this sequence still allowed satisfactory diagnostic confidence, which becomes of increasing importance given current concerns linking the administration of gadolinium chelates to nephrogenic systemic fibrosis in patients with severe renal impairment (33,34). As a consequence, several studies have focused attention on the minimization of gadolinium dose in risk patients. For future applications, a macrocyclic and high-relaxivity gadolinium-based contrast agent with a lower propensity to release gadolinium seems to be a more appropriate strategy. Furthermore, given the issue of nephrogenic systemic fibrosis, alternative techniques such as non-CE MRA or 3D dark-blood MRA must be considered (35). Nevertheless, a major limitation to parallel acquisition techniques is that SNR is decreased, mainly depending on the degree of k-space undersampling and coil geometry (24). Therefore at 1.5 T, SNR penalties usually limit the maximum acceleration factor to about 2 for most abdominal applications at 1.5 T (21,36).

Advantages of Higher Field Strength

Improved gradient performance and a higher baseline level of SNR at 3 T may help compensate for parallel imaging–related SNR loss, allowing faster acquisition with high imaging matrices (4,8,32,36). On the basis of these theoretical advantages, we implemented a time-resolved CE MR angiographic sequence using a high parallel imaging factor of 3 and an in-plane resolution of 1.1 × 0.8 mm, which is at least comparable to single-phase CE MRA.

Second, the longitudinal relaxation time (T1) of unenhanced blood and background tissue increases with field strength substantially. Therefore, fast repetitious radiofrequency excitations, as in the case of MR angiographic sequences, lead to an improved suppression of the background tissue because its relaxation rate is decreased. Accordingly, sensitivity to injected gadolinium agents for CE MRA is heightened at 3 T, adding the advantage of using less contrast material (21). In theory, the higher contrast agent efficacy allows reducing the administered amount of contrast without deteriorating image quality. Thus, in our study, time-resolved CE MRA was performed in addition to conventional single-phase high–spatial resolution CE MRA using only 3 to 5 mL of contrast. Possibly, the reduced amount of contrast might cause declined scores for vessel depiction when looking at the aortic branches. However, the small amount of contrast did not affect the high image quality of the aortoiliac (segments 1, 2, 10, and 11) and renal (segments 6 and 7) arteries. The remaining segments (aortic branches such as the hepatic artery or superior mesenteric artery) were outperformed by higher spatially resolved single-phase CE MRA.

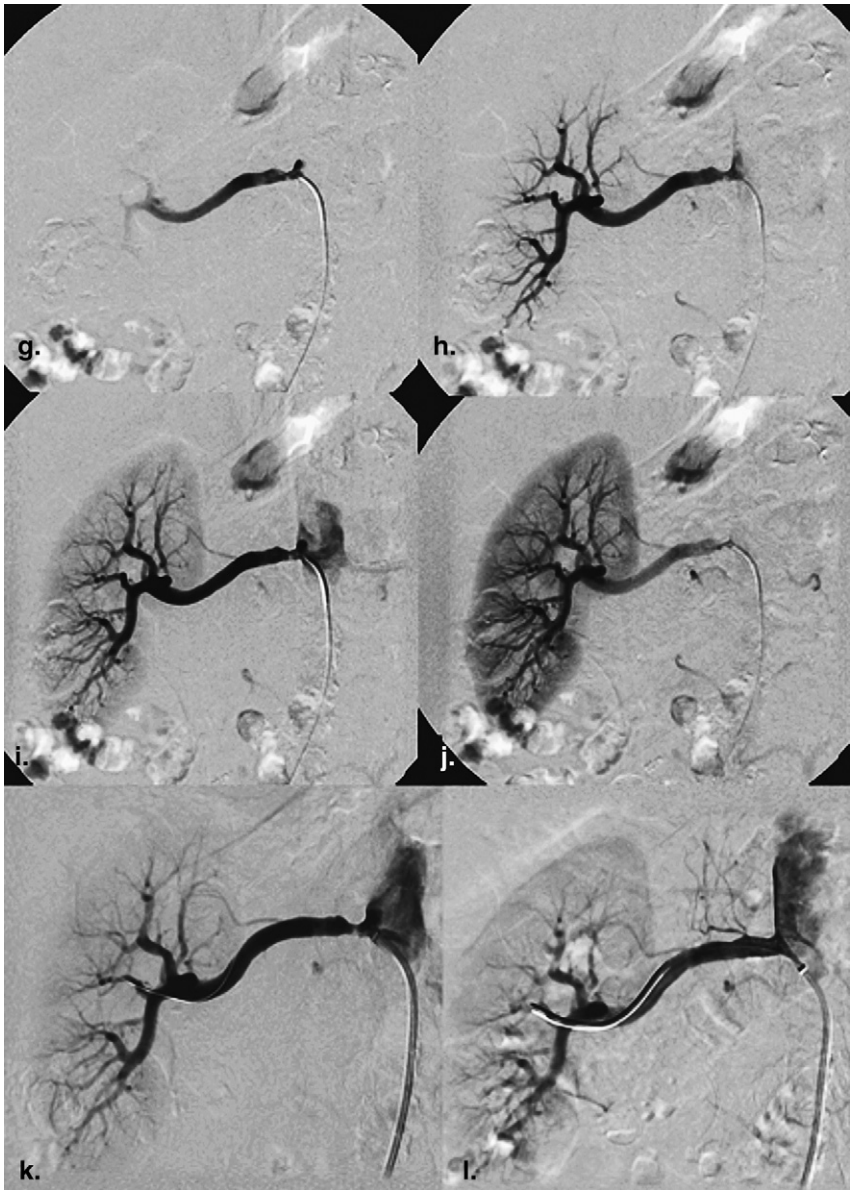

Figure 3. *(Continued)*

Potential Clinical Applications

Although time-resolved CE MRA cannot replace single-phase CE MRA when evaluating small-caliber abdominal branches, its addition to a standard abdominal MR protocol can provide useful dynamic information in conditions such as rapid parenchymal and/or venous enhancement, in which high–spatial resolution CE MRA may lack sufficient temporal resolution. The technique has potential value in the setting of renal stent placement for the assessment of altered hemodynamics, when stent-related susceptibility artifacts may limit anatomic evaluation, and could also be useful to assess hypervascular tumors, arteriovenous malformations, or arteriovenous fistulas. Several possible clinical applications have been established, including the evaluation of endoleaks in patients after aortoiliac endovascular aneurysm repair (37), the grading of RAS (12,38), or the evaluation of complex vascular anatomy prior to living kidney donation (31). Furthermore, in our study, contrast dynamics could be visualized in all cases with clear bolus-transit depiction, allowing the precise determination of individual circulation times. Volume coverage of the following single-phase high-resolution data sets could be checked easily. Another potential application will be the assessment of delayed parenchymal enhancement of the kidneys. In three patients, we were able to verify intermediate stenosis of the renal arteries by delayed parenchymal enhancement (see Fig 3).

Moreover, in patients with compromised respiratory function, time-resolved CE MRA might be valuable because of the acquisition times of <2 seconds per dynamic data acquisition. In contrast, even at higher field strength, using the progressive examination protocol mentioned above, breath-hold times up to 20 seconds are necessary for conventional

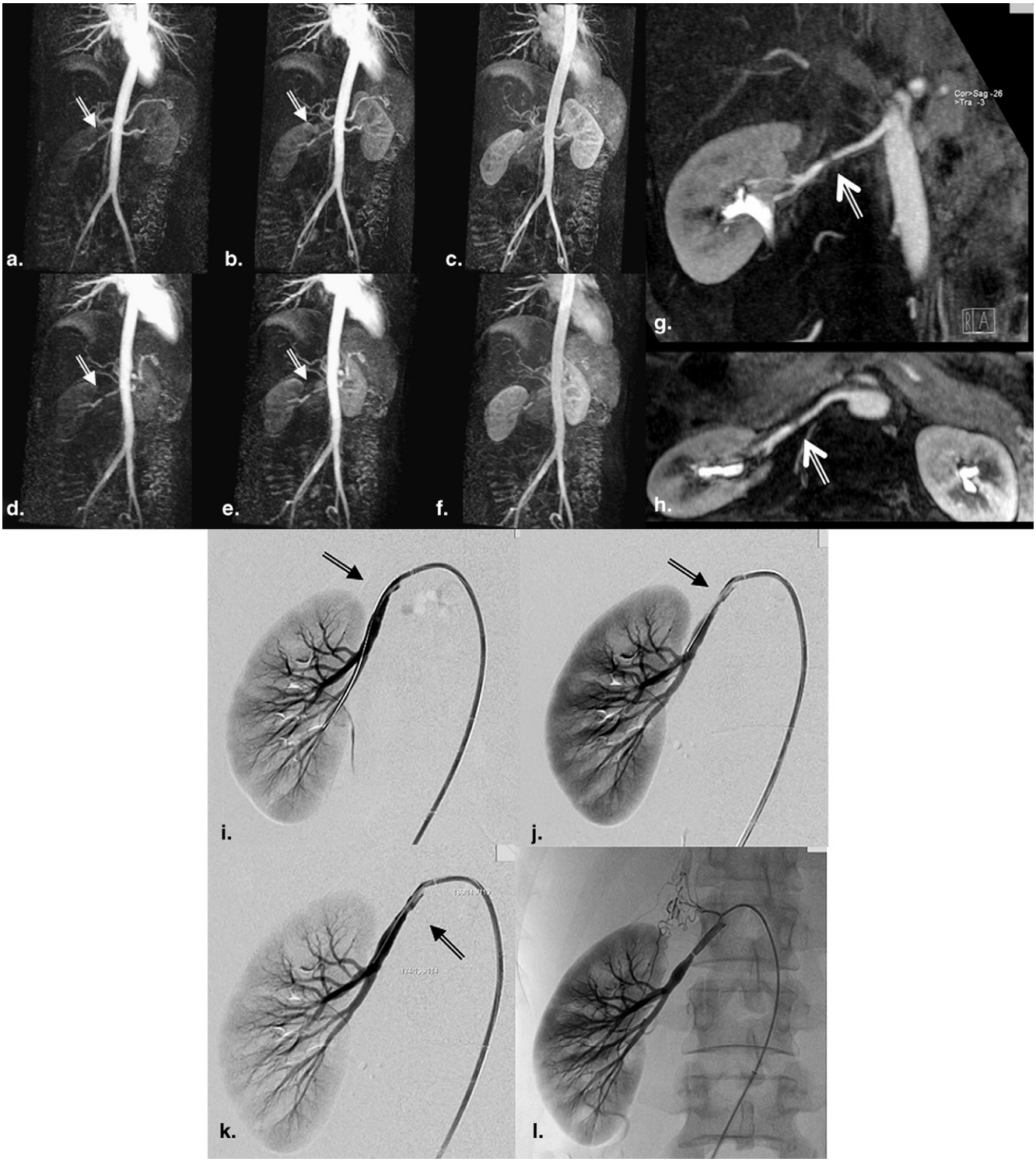

Figure 4. Six consecutive coronal time-resolved maximum-intensity projection images **(a–f)** in a 27-year-old woman patient presenting with a fibromuscular dysplasia–like lesion. Note the high-grade narrowing in the middle part of the right renal artery (white arrow), resulting in a delayed parenchymal enhancement of the right kidney. Findings were confirmed by coronal **(g)** and axial **(h)** reformats of high-resolution single-phase magnetic resonance angiography as well as by selective digital subtraction angiography **(i–l)**.

CE MRA of the entire abdominal aorta, and patients with liver disease or respiratory limitations are often not capable of holding their breath this long.

We were able to visualize the abdominal aorta and its major branches in all cases with high quality, as reported. Stenoses, occlusions, and aneurysms were correctly identified in seven

patients by time-resolved CE MRA. However, especially abdominal branches, such as the hepatic or splenic artery, primarily presenting with small vessel diameters even in healthy subjects, were visualized with less diagnostic confidence compared to conventional single-phase CE MRA. On the other hand, even on conventional CE MRA, these segments presented with inadequate arterial enhancement or impaired image quality in several cases compared to major branches such as the renal arteries (Table 3). However, finer vascular detail was significantly better appreciated on conventional CE MRA because of its higher spatial resolution relative to that of time-resolved CE MRA.

Image Postprocessing and Multiplanar Reformatting

Because of an increased slice thickness, the resolution of reformatted views obtained from time-resolved data sets is limited compared to single-phase CE MRA, although nonisotropic imaging can have high resolution in the imaged plane. This is significant because it has been shown that the sensitivity and specificity of abdominal CE MRA are greatly improved by viewing multiplanar reformats in addition to viewing the MIPs in the acquired plane (1,2,39). Because most arteries do not lie completely in the acquired plane, we speculate that an isotropic resolution of time-resolved CE MRA should prove very advantageous for reformatted images. In our study, time-resolved CE MRA was performed using a matrix size of 512 × 288, an interpolated slice thickness of 3.0 mm, and a true voxel size of 1.1 × 0.8 arteries 3.8 mm^3, which is still comparable to single-phase 3D CE MR angiographic acquisitions performed on a standard MR scanner operating at a field strength of 1.5 T (40). However, volume-rendered images derived from arterial data sets of time-resolved MR studies were suitable to obtain diagnostic image quality, even in complex vascular anatomy (Fig 5).

Limitations

There are acknowledged disadvantages of a loss of SNR from the parallel imaging (spatial undersampling) component and a trade-off between spatial and temporal resolution when temporal undersampling techniques are used. As a result of the limited spatial resolution of TWIST, diagnostic accuracy was restricted, often not allowing a reliable depiction of the anatomies of small arteries (eg, common hepatic artery, inferior mesenteric artery) in fine detail.

Second, the study was also limited by the lack of gold-standard correlation, because only four of the 22 patients underwent DSA; at our institution, management decisions are often based on ultrasound or MR angiographic findings, with DSA reserved for further evaluation or consideration of endovascular management. In consequence, the standard of reference used in this study was conventional high–spatial resolution CE MRA, and although it is known to be an imperfect standard, it is nonetheless an often performed screening test.

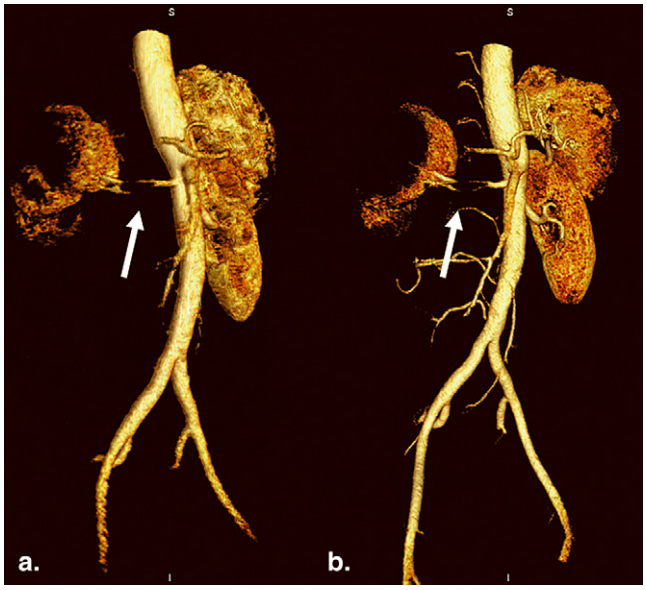

Figure 5. Rotated coronal volume-rendering technique images derived from time-resolved data set **(a)** and conventional single-phase magnetic resonance angiography **(b)**. There is a high-grade compression of the middle part of the right renal artery due to retroperitoneal, extravascular malignant tissue manifestation (with arrow). Delayed parenchymal enhancement can be observed on both images.

Third, another potential limitation related to the reduced spatial resolution of TWIST will be a less accurate stenosis severity estimation in calcified vasculature or after vascular intervention (eg, stent placement).

Fourth, we did not aim to calculate sensitivity and specificity in this study. Therefore, the accuracy of time-resolved CE MRA compared to that of single-phase CE MRA could not be assessed.

Finally, no separate analysis of oblique reformats compared to standard views (coronal and sagittal) in the assessment of fine vascular details was done.

For the aforementioned reasons and on the basis of our study results, we are proposing this technique not as a sole diagnostic tool but rather as a supplement to a high–spatial resolution acquisition. Therefore, it may be used to measure circulation times (eg, for conventional high–spatial resolution CE MRA) or to assess contrast material kinetics (3,4). In patients with limited breath-hold capabilities, TWIST can be accounted as a reliable alternative to single-phase CE MRA, thereby offering spatial resolution comparable to or even better than several published data concerning abdominal CE MRA at 1.5 T.

CONCLUSION

Time-resolved MRA using a low contrast dose yields rapid and important anatomic and functional information for the assessment of the abdominal vasculature with both good spatial resolution and a high temporal reconstructed frame rate. In our opinion, time-resolved abdominal MRA might

be particularly useful in patients with limited breath-hold capabilities or when limiting contrast dose is desirable. However, because of decreased spatial resolution, time-resolved MRA is inferior to conventional high–spatial resolution CE MRA in demonstrating fine vascular details.

REFERENCES

1. De Cobelli F, Venturini M, Vanzulli A, et al. Renal arterial stenosis: prospective comparison of color Doppler US and breath-hold, three-dimensional, dynamic, gadolinium-enhanced MR angiography. Radiology 2000; 214: 373–380.
2. Fain SB, King BF, Breen JF, et al. High-spatial-resolution contrast-enhanced MR angiography of the renal arteries: a prospective comparison with digital subtraction angiography. Radiology 2001; 218: 481–490.
3. Leung DA, Hagspiel KD, Angle JF, et al. MR angiography of the renal arteries. Radiol Clin North Am 2002; 40:847–865.
4. Fenchel M, Nael K, Deshpande VS, et al. Renal magnetic resonance angiography at 3.0 Tesla using a 32-element phased-array coil system and parallel imaging in 2 directions. Invest Radiol 2006; 41:697–703.
5. Nael K, Saleh R, Lee M, et al. High-spatial-resolution contrast-enhanced MR angiography of abdominal arteries with parallel acquisition at 3.0 T: initial experience in 32 patients. AJR Am J Roentgenol 2006; 187: W77–W85.
6. Schoenberg SO, Rieger J, Weber CH, et al. High-spatial-resolution MR angiography of renal arteries with integrated parallel acquisitions: comparison with digital subtraction angiography and US. Radiology 2005; 235: 687–698.
7. Zhang H, Prince MR. Renal MR angiography. Magn Reson Imaging Clin N Am 2004; 12:487–503.
8. Kramer U, Wiskirchen J, Fenchel MC, et al. Isotropic high-spatial-resolution contrast-enhanced 3.0-T MR angiography in patients suspected of having renal artery stenosis. Radiology 2008; 247: 228–240.
9. Leung DA, Hany TF, Debatin JF. Three-dimensional contrast-enhanced magnetic resonance angiography of the abdominal arterial system. Cardiovasc Intervent Radiol 1998; 21:1–10.
10. Michaely HJ, Nael K, Schoenberg SO, et al. The feasibility of spatial high-resolution magnetic resonance angiography (MRA) of the renal arteries at 3.0 T. Rofo 2005; 177:800–804.
11. Wilson GJ, Hoogeveen RM, Willinek WA, Muthupillai R, Maki JH. Parallel imaging in MR angiography. Top Magn Reson Imaging 2004; 15:169–185.
12. Schoenberg SO, Bock M, Knopp MV, et al. Renal arteries: optimization of three-dimensional gadolinium-enhanced MR angiography with bolus-timing-independent fast multiphase acquisition in a single breath hold. Radiology 1999; 211:667–679.
13. Shetty AN, Bis KG, Kirsch M, et al. Contrast-enhanced breath-hold three-dimensional magnetic resonance angiography in the evaluation of renal arteries: optimization of technique and pitfalls. J Magn Reson Imaging 2000; 12:912–923.
14. Prince MR, Chenevert TL, Foo TK, et al. Contrast-enhanced abdominal MR angiography: optimization of imaging delay time by automating the detection of contrast material arrival in the aorta. Radiology 1997; 203: 109–114.
15. Wilman AH, Riederer SJ, King BF, et al. Fluoroscopically triggered contrast-enhanced three-dimensional MR angiography with elliptical centric view order: application to the renal arteries. Radiology 1997; 205: 137–146.
16. Fenchel M, Saleh R, Dinh H, et al. Juvenile and adult congenital heart disease: time-resolved 3D contrast-enhanced MR angiography. Radiology 2007; 244:399–410.
17. Korosec FR, Frayne R, Grist TM, Mistretta CA. Time-resolved contrast-enhanced 3D MR angiography. Magn Reson Med 1996; 36: 345–351.
18. Pinto C, Hickey R, Carroll TJ, et al. Time-resolved MR angiography with generalized autocalibrating partially parallel acquisition and time-resolved echo-sharing angiographic technique for hemodialysis arteriovenous fistulas and grafts. J Vasc Interv Radiol 2006; 17:1003–1009.
19. Mistretta CA, Grist TM, Korosec FR, et al. 3D time-resolved contrast-enhanced MR DSA: advantages and tradeoffs. Magn Reson Med 1998; 40:571–581.
20. Michaely HJ, Herrmann KA, Kramer H, et al. High-resolution renal MRA: comparison of image quality and vessel depiction with different parallel imaging acceleration factors. J Magn Reson Imaging 2006; 24:95–100.
21. Kramer U, Nael K, Laub G, et al. High-resolution magnetic resonance angiography of the renal arteries using parallel imaging acquisition techniques at 3.0 T: initial experience. Invest Radiol 2006; 41:125–132.
22. Griswold MA, Jakob PM, Heidemann RM, et al. Generalized autocalibrating partially parallel acquisitions (GRAPPA). Magn Reson Med 2002; 47: 1202–1210.
23. Pruessmann KP, Weiger M, Scheidegger MB, Boesiger P. SENSE: sensitivity encoding for fast MRI. Magn Reson Med 1999; 42:952–962.
24. Werder R, Nanz D, Lutz AM, et al. Assessment of the abdominal aorta and its visceral branches by contrast-enhanced dynamic volumetric hepatic parallel magnetic resonance imaging: feasibility, reliability and accuracy. Eur Radiol 2007; 17:541–551.
25. Nael K, Michaely HJ, Lee M, et al. Dynamic pulmonary perfusion and flow quantification with MR imaging, 3.0T vs. 1.5T: initial results. J Magn Reson Imaging 2006; 24:333–339.
26. Swan JS, Carroll TJ, Kennell TW, et al. Time-resolved three-dimensional contrast-enhanced MR angiography of the peripheral vessels. Radiology 2002; 225:43–52.
27. Kramer H, Michaely HJ, Requardt M, et al. Effects of injection rate and dose on image quality in time-resolved magnetic resonance angiography (MRA) by using 1.0M contrast agents. Eur Radiol 2007; 17: 1394–1402.
28. Du J, Fain SB, Korosec FR, et al. Time-resolved contrast-enhanced carotid imaging using undersampled projection reconstruction acquisition. J Magn Reson Imaging 2007; 25:1093–1099.
29. Wieben O, Grist TM, Hany TF, et al. Time-resolved 3D MR angiography of the abdomen with a real-time system. Magn Reson Med 2004; 52: 921–926.
30. Nael K, Ruehm SG, Michaely HJ, et al. High spatial-resolution CE-MRA of the carotid circulation with parallel imaging: comparison of image quality between 2 different acceleration factors at 3.0 Tesla. Invest Radiol 2006; 41:391–399.
31. Kramer U, Thiel C, Seeger A, et al. Preoperative evaluation of potential living related kidney donors with high-spatial-resolution magnetic resonance (MR) angiography at 3 Tesla: comparison with intraoperative findings. Invest Radiol 2007; 42:747–755.
32. Campeau NG, Huston J III, Bernstein MA, et al. Magnetic resonance angiography at 3.0 Tesla: initial clinical experience. Top Magn Reson Imaging 2001; 12:183–204.
33. Grobner T. Gadolinium—a specific trigger for the development of nephrogenic fibrosing dermopathy and nephrogenic systemic fibrosis? Nephrol Dial Transplant 2006; 21:1104–1108.
34. Perez-Rodriguez J, Lai S, Ehst BD, et al. Nephrogenic systemic fibrosis: incidence, associations, and effect of risk factor assessment—report of 33 cases. Radiology 2009; 250:371–377.
35. Mihai G, Chung YC, Kariisa M, et al. Initial feasibility of a multi-station high resolution three-dimensional dark blood angiography protocol for the assessment of peripheral arterial disease. J Magn Reson Imaging 2009; 30:785–793.
36. Michaely HJ, Kramer H, Dietrich O, et al. Intraindividual comparison of high-spatial-resolution abdominal MR angiography at 1.5 T and 3.0 T: initial experience. Radiology 2007; 244:907–913.
37. Cohen EI, Weinreb DB, Siegelbaum RH, et al. Time-resolved MR angiography for the classification of endoleaks after endovascular aneurysm repair. J Magn Reson Imaging 2008; 27:500–503.
38. Volk M, Strotzer M, Lenhart M, et al. Time-resolved contrast-enhanced MR angiography of renal artery stenosis: diagnostic accuracy and interobserver variability. AJR Am J Roentgenol 2000; 174:1583–1588.
39. Baskaran V, Pereles FS, Nemcek AA Jr, et al. Gadolinium-enhanced 3D MR angiography of renal artery stenosis: a pilot comparison of maximum intensity projection, multiplanar reformatting, and 3D volume-rendering postprocessing algorithms. Acad Radiol 2002; 9:50–59.
40. Vasbinder GB, Nelemans PJ, Kessels AG, et al. Accuracy of computed tomographic angiography and magnetic resonance angiography for diagnosing renal artery stenosis. Ann Intern Med 2004; 141:674–682.